

Investigation of the secondary electron emission characteristics of alternative dynode materials for imaging photomultipliers

This article has been downloaded from IOPscience. Please scroll down to see the full text article.

2012 JINST 7 C03018

(<http://iopscience.iop.org/1748-0221/7/03/C03018>)

View [the table of contents for this issue](#), or go to the [journal homepage](#) for more

Download details:

IP Address: 137.222.43.33

The article was downloaded on 06/06/2012 at 16:57

Please note that [terms and conditions apply](#).

THE 9th INTERNATIONAL CONFERENCE ON POSITION SENSITIVE DETECTORS,
12–16 SEPTEMBER 2011,
ABERYSTWYTH, U.K.

Investigation of the secondary electron emission characteristics of alternative dynode materials for imaging photomultipliers

J.S. Lapington,^{a,1} V. Taillandier,^a B.L. Cann,^a J. Howorth^b and J. Milnes^b

^aSpace Research Centre, University of Leicester, University Road, Leicester, LE1 7RH, U.K.

^bPhotek Ltd., 26 Castleham Road, St. Leonards on Sea, East Sussex, TN38 9NS, U.K.

E-mail: jsl12@star.le.ac.uk

ABSTRACT: The requirement to accurately detect and image very high speed photon events is a necessity for many applications across a range of disciplines. Photon imaging detectors often make use of the planar geometry of MCPs for high resolution imaging. However, the inherent rate limitations of MCPs provide opportunities for discrete dynode devices where rapid recharge times and high throughput are required.

Novel dynode materials and designs offer the possibility to further improve event time resolution and pulse height distribution. Significant performance advantages can be achieved by increasing the gain of each dynode stage by utilizing materials such as CVD diamond. Secondary electron emission (SEE) coefficients for polycrystalline CVD diamond of 84 have been reported for Hydrogen terminated surfaces and similar values for Cs terminated surfaces [1, 2]. These values are far in excess of currently used materials such as AgMgO(Cs) and CuBeO(Cs) which have SEE coefficients < 15 [3].

Polycrystalline diamond is a widely available, relatively inexpensive material that can be deposited over large areas, making the manufacture of large format imaging detectors a practical possibility. The application of new dynode designs for imaging photomultipliers requires knowledge of the secondary electron emission characteristics of the material. We describe a facility to measure the relevant characteristics of novel dynode materials and designs with 2D imaging capability, and discuss the challenges and complexities involved with SEE coefficient measurements. We present secondary electron emission measurements for a variety of dynode materials and designs and discuss their application in imaging photon-counting devices.

KEYWORDS: Secondary electron emitters and dynodes and their production; Electron multipliers (vacuum)

¹Corresponding author.

Contents

1	Introduction	1
1.1	Diamond attributes	2
2	Experimental apparatus	3
2.1	SEE measurement facility	3
2.2	Photek measurement tubes	4
2.3	Samples	5
3	Design and operation	6
3.1	Features	6
3.2	Measurement issues	6
4	Results	7
4.1	SEE measurements	8
4.1.1	SEE uniformity	10
4.1.2	Variation in sample thickness	10
4.1.3	Test cell determined SEE coefficients	11
5	Discussion	12
5.1	Apparatus	12
5.2	Low peak SEE energy	13
5.3	SEE uniformity	14
5.4	Boron concentration	14
5.5	Sample thickness	15
5.6	Test cell measurements	15
6	Conclusions	15

1 Introduction

Accurate detection of photon events at very high speed is a requirement in many applications. If single photon counting is a requirement, signal amplification mechanism is essential. The photomultiplier tube (PMT), developed in the 1930's, was the first device to utilize *in vacuo* electronic signal amplification and has been a workhorse detector for high speed, high sensitivity and photon counting applications ever since. Another device utilizing *in vacuo* electron amplification is the microchannel plate (MCP), a planar array of miniaturized pores each acting as a continuous dynode surface, which can achieve event timing in the 10's of picoseconds regime and high resolution imaging limited by the MCP granularity.

A determining factor in the performance and complexity of *in vacuo* electron gain devices is the secondary electron emission (SEE) coefficient of the dynode surface, i.e. the number of secondary electrons produced per primary electron impacting the dynode surface. In multistage devices the gain progression is geometric, the overall gain being the product of the gain per stage over all gain stages. Increased SEE allows the number of gain stages to be reduced, and increases the likelihood that an initial photoelectron gives rise to a detectable event, improving overall efficiency. Boron-doped polycrystalline diamond film deposited using chemical vapour deposition (CVD) techniques has been shown to exhibit significantly enhanced SEE compared to traditional dynode materials, and offers other significant advantages as well.

1.1 Diamond attributes

CVD Diamond has unique SEE characteristics with yields of >80 at 3 keV reported [1, 2]. This behaviour results from a combination of excellent electron transport properties and the possibility of negative electron affinity (NEA) of a suitably terminated surface. The energy of an incoming primary electron produces low energy secondary electrons, located close to the conduction band minimum, and distributed within the bulk of the material. In the secondary electron transport phase diamond's wide band gap (5.47 eV) and relatively low density of conduction band electrons limit the available inelastic scattering processes, and thus energy loss, allowing a large escape depth. Having reached the surface, a large proportion of these low energy electrons can escape due to the NEA characteristic of the surface. Diamond surfaces have been shown to exhibit NEA when terminated using hydrogen and alkali metals such as caesium [1]. The wide band gap of diamond also effectively eliminates thermal noise at typical operating temperatures.

The higher gain per stage due to increased SEE results in a lower number of stages for a given gain, an advantage in terms of device size, cost, and complexity. Higher gain per stage does require an increased voltage. However, the Poisson statistics at higher gains (particularly at the first stage) produce an intrinsically narrower pulse height distribution (PHD) which can improve signal to noise ratio, allowing the detector to be operated at lower overall gain. The narrower PHD also provides improved energy resolution for scintillation counters where the number of simultaneously detected photons is required.

CVD diamond deposition uses relatively standard CVD equipment. Thin polycrystalline films are straightforwardly grown on single crystal silicon wafer material and do not require lattice matched substrates as do some other high SEE materials. Diamond has a relatively stable SEE, little affected by long term storage so long as surface contamination is avoided. High SEE diamond surfaces are air-stable, and can be reactivated by surface re-termination following ageing due to charge extraction.

The CVD diamond material analysis task described here is one element of a project to develop diamond dynode-based photomultipliers for high speed imaging, with collaborators at the Diamond Group at the University of Bristol, the Micro and Nanotechnology Centre at the Rutherford Appleton Laboratory, and the Atomic Weapons Establishment, UK. We have developed, refined, and verified a facility to measure a variety of CVD diamond samples produced with a variety of crystal sizes, dopant concentrations, film thicknesses, substrate materials, nucleation methods, etc. We have measured the SEE, uniformity, lifetime, and other properties pertinent to photomultiplier dynode material. Samples have also been tested by incorporation in vacuum phototriode tubes.

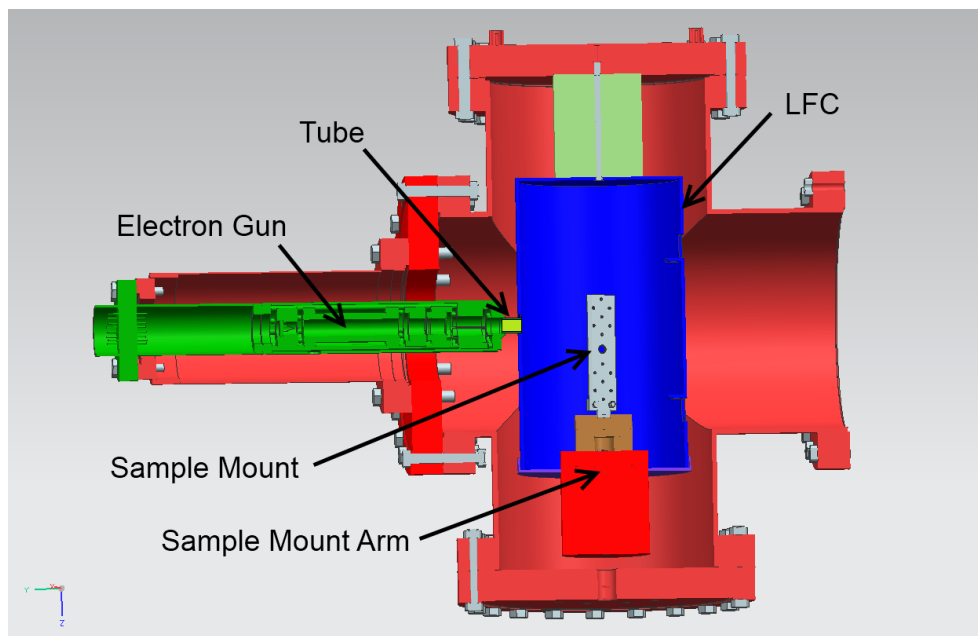


Figure 1. A cross section through the experimental apparatus used for secondary electron emission measurements.

2 Experimental apparatus

2.1 SEE measurement facility

The apparatus comprises a bakeable, stainless steel vacuum chamber with internal custom electrodes, heaters and thermocouples, a remotely controlled electron gun, several precision electrometers, a data acquisition PC, and an oil-free high vacuum turbo pump set with gauges.

The cruciform vacuum chamber contains an inner, insulated charge containment cylinder concentric with the chamber, known as the Large Faraday Cup (LFC). The LFC contains a centrally mounted, electrically insulated, conductive sample support arm which can be moved laterally by ± 25 mm and rotated 360° around its axis. This lateral motion allows for up to four 1cm square samples and a small Faraday cup (SFC) to be positioned in the line of the primary electron beam. The electron beam is orthogonal to the LFC and sample arm axis. The electron gun and electrical feed-throughs for current measurement signals, thermocouples, and heater power supply are mounted on conflat vacuum flanges. A quartz halogen lamp, mounted within the LFC, provides bake-out capability and potential to operate at elevated temperatures.

The sample arm and electron beam enter the LFC through shielded apertures. The electron beam from the electron gun enters the LFC through an insulated aluminium tube (which can be independently biased and is used for diagnostics) towards the target arm. The sample arm supports the material to be measured and also houses the small Faraday cup (SFC) which can be configured with different aperture sizes (0.5–0.05 mm ID) for beam focus diagnostics. A semi-circular stainless steel shim behind the sample arm was used as an electron collector. It can either be electrically isolated for transmission measurements or connected to the sample arm and act as the SFC internal volume. A schematic of the apparatus is shown in figure 1.

The ELS5000 electron gun, manufactured by PSP Vacuum Technology [4], produces a focussed electron beam with a spot size down to 50 μm , a beam current of 10nA–10 μA , at a working distance of ~ 67 mm, and a beam energy from 0.25 to 5keV. The electron gun has in-built electrostatic deflection which can position the beam ± 4 mm off-axis in the xy plane. This is used to image the SEE across the sample.

Secondary electrons escaping from the sample surface, which comprise low energy secondaries, and elastic and inelastically scattered primaries, are collected by the LFC. The original stainless steel LFC was remanufactured in mu-metal to eliminate external magnetic fields which initially caused beam deflection and imaging ambiguities. The beam focus is optimised by positioning it directly over the SFC aperture and adjusting to minimise measured SEE. The minimum value occurs when the beam is tightest and thus focussed through the SFC. The beam profile can also be measured by rastering it over the SFC aperture and measuring sample and LFC currents.

The LFC, sample arm (collector when required) and tube can be individually biased and their currents measured independently. Keithley 6514 and 6517B electrometers and a 6485 Picoammeter were used, operated as precision ammeters.

The electron beam current is calibrated by two methods:

1. The beam can be collected completely in the SFC, the sample current equalling the beam current, confirmed by a zero LFC current, and
2. The beam current can be calculated from the sum of the currents on all electrodes.

Method 1 requires the electron beam to be sufficiently well focussed to completely enter the SFC aperture.

The SEE coefficient in reflection (SEE_R) is calculated by the following expressions for methods 1 and 2 respectively:

$$SEE_R = \left(= \frac{I_{\text{out}}}{I_{\text{out}} + I_{\text{in}}} \right) = \frac{I_{\text{LFC}}}{I_{\text{SFC}}} = \frac{I_{\text{LFC}}}{I_{\text{LFC}} + I_{\text{Target}}} \quad (2.1)$$

where: I_{LFC} is the LFC current, I_{Target} is the sample or target current, and I_{SFC} is the SFC current (measured separately). The second method is generally used because it is intrinsic to the measurements and is independent of electron beam fluctuations. Comparison of the two methods indicates they agree to within $< 10\%$.

The SEE in transmission (SEE_T) is calculated using:

$$SEE_T = \frac{I_{\text{Collector}}}{I_{\text{LFC}} + I_{\text{Target}} + I_{\text{Collector}}} \quad (2.2)$$

2.2 Photek measurement tubes

SEE_R coefficients have also been measured at Photek using demountable and photo-tube configurations (see figure 2). In the demountable configuration the electron source is a filament whereas the photo-tube uses a calibrated photocathode. In both configurations a small aperture controls the illuminated area, which is negatively biased with respect to the diamond sample. A mesh between the aperture and the diamond sample is positively biased with respect to the sample to collect the secondary electrons. The sample is mounted on a spring clip in the case of the demountable, or spot

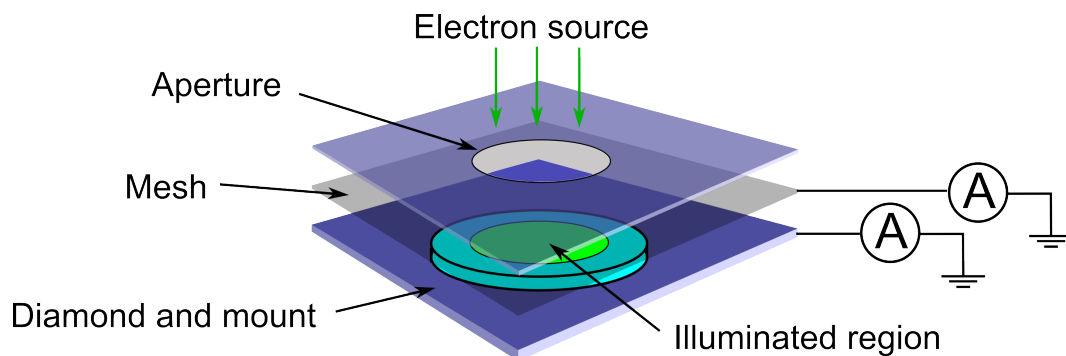


Figure 2. A schematic of the experimental configuration of the demountable phototube used to measure *SEE*.

welded with nickel tape to a kovar plate in the photo-tube. The mesh and sample mount currents are measured and the *SEE* ratio is calculated from (2.1). In the de-mountable the incident current, I_{in} , is the diamond current with the mesh biased negative. In the photo-tube configuration the I_{in} is calculated using the photocathode calibration.

2.3 Samples

Diamond samples have been obtained from three independent suppliers; Bristol University Diamond Group (manufactured specifically for the project), Diamond Detectors Limited and Genvac Aerospace Inc. Samples grown at Bristol University are polycrystalline diamond films with various thicknesses and boron doping levels. Micro and nano-crystalline diamond (MCD and NCD) films have been grown on monocrystalline (100) oriented silicon and molybdenum substrates by a CVD method in a hot filament diamond reactor [5]. A number of samples from Genvac Aerospace Inc. have been measured. These are MCD films grown on Molybdenum substrates, however no further specification is available. Diamond Detectors Ltd (DDL) supplied four free standing samples grown by Element Six with polycrystalline grain sizes $\sim 50 \mu\text{m}$.

1. Sample A: “premium detector grade polycrystalline” intrinsic diamond, $3 \times 3 \times 0.3 \text{ mm}^3$, very highly polished on both sides ($< 4 \text{ nm}$).
2. Sample B: “standard detector grade polycrystalline” intrinsic diamond, $5 \times 5 \times 0.5 \text{ mm}^3$, polished to a $< 4 \text{ nm}$ RMA roughness on one side and left unpolished on the other.
3. Sample C: high purity single crystal intrinsic diamond plate $5 \times 5 \times 0.2 \text{ mm}^3$, polished both sides to $< 4 \text{ nm}$ RMA roughness.
4. Sample D: $10 \times 10 \times 0.5 \text{ mm}^3$ boron doped to $> 10^{20}$ boron atoms per cm^3 , polished one side to $< 12 \text{ nm}$ RMA roughness and lapped on the other side.

Intrinsic samples had an additional layer of boron doped diamond deposited onto specific sample faces to provide a recharge current path while maintaining crystallite geometry. The unpolished surface of sample B and both surfaces of sample C were coated with a layer of boron doped diamond $1 \mu\text{m}$ thick using residual doping and MCD growth conditions, but without seeding / manual

abrasion. In this case residual doping refers to the growth of diamond with no deliberate doping, any uptake in boron resulting from residual chamber contamination. The samples were hydrogen terminated by exposure to atomic hydrogen in the CVD chamber for 5 minutes after growth.

3 Design and operation

3.1 Features

The experimental apparatus has the following features:

1. The capability to image the sample SEE over $8 \times 8 \text{ mm}^2$ for uniformity measurement.
2. The SEE is calculated using the sum of target and LFC currents for primary beam current. This avoids error due to drift in the beam current, but is sensitive to electron loss from the system especially at high values of SEE. Measurement of the beam current directly using the SFC is used for corroboration.
3. The ability to test large area transmissive dynode and multi-dynode imaging structures.

Measurement of SEE can be undertaken in pulsed and continuous electron beam modes. In previous work [6] we have reported pulsed mode measurements, but for the SEE imaging reported here continuous illumination was used with 0.6 s dwell at each measurement point.

Variation of SEE over time can affect both measurement modes. It has been shown [7] that electron bombardment degrades the SEE coefficient through hydrogen desorption over relatively long timescales, however we have also observed SEE enhancement and degradation effects over shorter timescales, which have also been reported elsewhere [8].

3.2 Measurement issues

Initial measurements exhibited an image shift and scale change when the electron beam energy was varied. This was problematic since reliable SEE versus position data for uniformity studies required accurate coordinate mapping between different energies. Since this could only be provided by image registration, samples had to be imaged at every energy which could result in premature ageing due to charge extraction. It had already been noted that image shifts were produced by extraneous operations, including placement of metallic objects outside the chamber, and so stray magnetic field influence was suspected. The observed image movement was greatly reduced by shielding the electron gun and remanufacturing the LFC with mu-metal components.

We primarily use the total measured current as a measure of instantaneous beam current. When measuring high SEE material, the target and LFC currents are of opposite sign and much larger than the beam current itself. In these circumstances loss of a small fraction of the secondary electron current causes the calculated beam current to be under-estimated producing an over-estimation of the SEE. Much effort has been made to reduce the possibility that secondary electron loss can occur, and the independent measurement of beam current by means of the SFC used as a diagnostic of success. Measures taken have included the addition of geometric shielding to eliminate possible electron loss paths to the chamber, establishment of the electrode biasing regime, and the addition of extra electrodes as diagnostic aids.

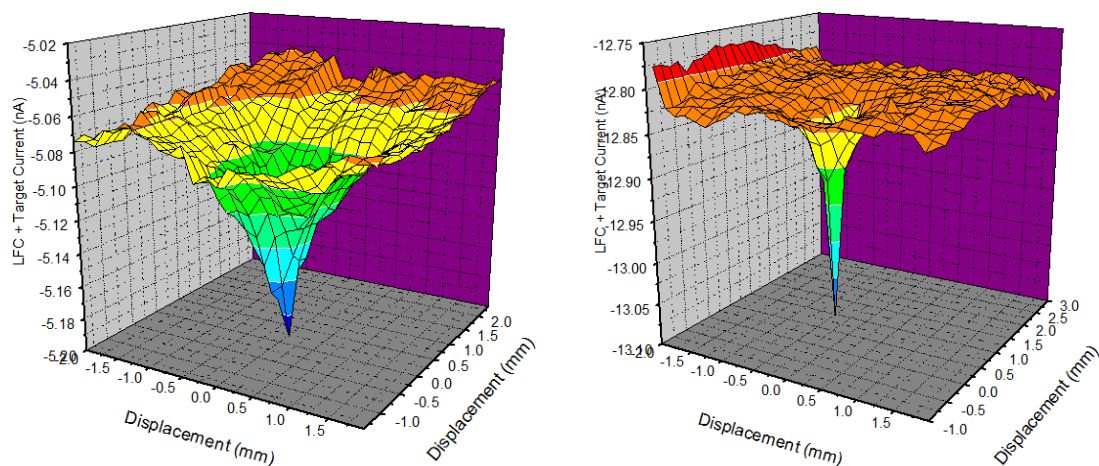


Figure 3. The ‘on-axis’ feature, observed in the LFC + target currents, is displayed in 3D perspective plots, with the primary beam energy at (a) 0.25 kV and (b) 2 kV on the left and right respectively. The shape of the feature sharpens with increasing beam energy.

The biasing regime is typically: all electrodes held at 0V apart from the LFC at +80V. Biasing was found to be especially important when a quartz lamp for sample heating was mounted within the LFC, opposite the electron beam entrance aperture. The presence of the lamp (not in operation and with its electrodes connected to the LFC) in an unbiased system significantly affected the measured total current, suggesting that charge up of the glass envelope sufficiently perturbed the low energy secondary electron trajectories allowing them to escape measurement, and effectively be lost to the chamber walls.

The addition of the tube at the nose of the electron gun helped to resolve the feature shown in figure 3, a peaked increase in electron beam current centred on the gun axis whose width varied with beam energy. This was eventually identified as a lower energy beam component, probably derived from secondary electrons produced from an accelerating mesh. These are apparent as the peaked feature in figure 3 with the beam on-axis, but recaptured within the gun when the beam is electrostatically deflected off-axis to an extent which varies as a function of beam energy. The extra tube electrode was used to successfully mitigate this feature of the electron gun.

4 Results

One of the main motivations to use diamond as a photomultiplier dynode is its high gain potential. SEE figures for CVD diamond in the published literature vary widely for nominally similar hydrogen terminated material, with the highest values reported being ~ 25 at 1 keV and linearly rising towards 3 keV [1, 2]. In order to arrive at the recipe for an ‘ideal’ material specification for our application we have measured samples with a range of boron concentrations, thicknesses, terminations, substrate materials and crystallite size ranges to optimise relevant performance characteristics. Initially even our own observations produced varied results revealing little in the way of patterns or trends. These discouraging results made us suspect our experimental setup so we undertook an organized investigation of possible contributing factors. Several effects were identified

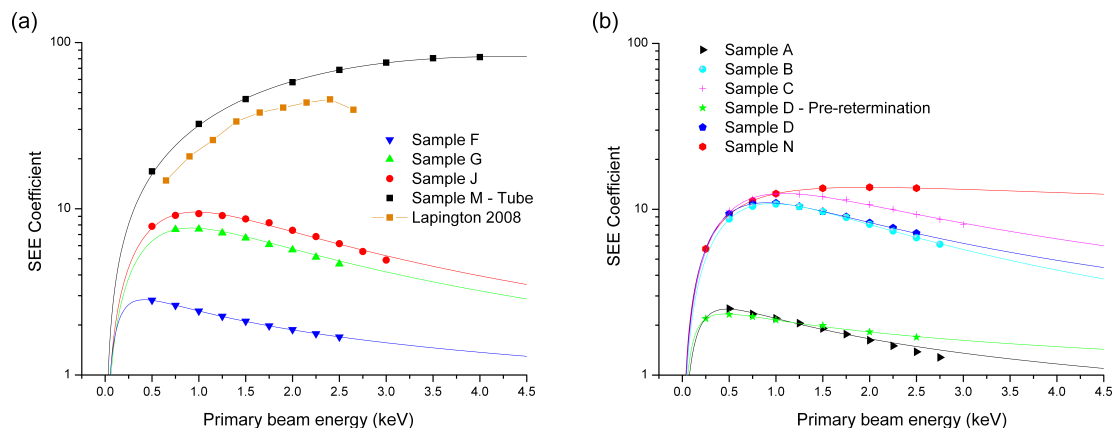


Figure 4. SEE coefficients plotted against primary beam energy. Points represent experimental data and the lines, fitted data using the expression (3). Plot (a) shows samples from our Bristol colleagues measured at Leicester (F, G and J) and sample M tested at Photek (data from [6] is shown for comparison), and plot (b), samples from DDL and Genvac (N).

and corrected as discussed in the previous section, however the basic approach proved sound, and the facility is operating repeatably and reliably.

Secondary electron emission is extremely sensitive to surface quality. Contamination was investigated using Secondary Ion Mass Spectroscopy (SIMS) and significant concentrations of the contaminant Polydimethylsiloxane (PDMS) [9] were observed on samples transported in ‘GelPack’, membrane boxes and when low density polyethylene (bubble wrap) was present within the transport container. Although this was not directly identified as affecting SEE, metallic boxes and sample mounts were used from then on. Also at this stage the majority of samples were re-terminated which generally, though not universally, improved the SEE.

4.1 SEE measurements

Here we report on a subset of samples which have been re-hydrogen terminated: the full suite will be reported on at a later date. We have measured samples from different suppliers, with varying crystallite sizes from nano-crystalline to single crystal, boron dopant concentrations in the range 10^{19} – 10^{21} /cm³, film thicknesses from 200 nm to 5 μ m, free-standing and deposited on silicon and molybdenum substrates.

As yet we have not consistently achieved the remarkable results reported elsewhere [2] but have observed moderate average SEE coefficients measured over large areas. The samples were measured at a pressure of $\sim 10^{-7}$ Torr, after hydrogen termination and subsequent exposure to air but with no additional treatment. The material and measurement parameters are given in table 1.

The fitted lines in figure 4 were generated using the $SEE(E)$ expression given by [10].

$$SEE = SEE_{pk} \frac{s \times \left(\frac{E}{E_{SEEpk}} \right)}{s - 1 + \left(\frac{E}{E_{SEEpk}} \right)^s} \quad (4.1)$$

where SEE is the secondary electron emission coefficient, E is the electron beam energy, s is a fit parameter, SEE_{pk} is the peak SEE, and E_{SEEpk} is the electron beam energy at SEE_{pk} . Best fits were obtained using a least squares fitting routine.

Table 1. SEE coefficients for measured samples. Measurements are averages over a user defined area. Resulting standard deviations from the mean are quoted as absolute values and as a percentage of the mean. The diamond type is either Nano- or Micro-Crystalline Diamond (NCD, MCD). L Indicates large crystallites of order $50\ \mu\text{m}$, SC indicates a single crystal sample, NC indicates not completed, UK indicates unknown, pk indicates peak rather than average, RD indicates that $1\ \mu\text{m}$ of residually doped diamond has been deposited on the intrinsic diamond substrate.

<i>Sample</i>	<i>Diamond type</i>	<i>Supplier</i>	<i>Average SEE</i>	<i>Boron conc.</i>	<i>Thickness (μm)</i>	<i>SEE SD</i>	<i>SD % of mean</i>	<i>Average Area (mm^2)</i>
<i>A — DDL polished</i>	MCD(L)	DDL	2.5	RD	500	0.03	1.11	1.9
<i>B — DDL unpolished</i>	MCD(L)	DDL	10.5	RD	500	0.21	2.01	7.4
<i>C — DDL SC</i>	SC	DDL	12.3	RD	500	0.21	1.74	3.9
<i>D — DBB DDL</i>	MCD(L)	DDL	11.5	$< 10^{20}$	500	1.38	12.04	26.2
<i>E — S02.11</i>	NCD	Bristol	2.7	7×10^{19}	1.5	0.23	8.41	17.7
<i>F — S02.12</i>	NCD	Bristol	3.0	4×10^{18}	1.5	0.19	6.32	19.7
<i>G — S02.1</i>	NCD	Bristol	7.6	2×10^{20}	3.5	0.14	1.78	8.7
<i>H — S02.6</i>	NCD	Bristol	8.0	2×10^{21}	3.5	0.31	3.85	12.6
<i>I — S02.8</i>	NCD	Bristol	7.0	1×10^{21}	3.5	0.24	3.41	7.1
<i>J — S01.0</i>	MCD	Bristol	9.2	0*	3.5	0.29	3.18	9.1
<i>K — S01.1</i>	MCD	Bristol	8.5	3×10^{19}	2.25	0.26	3.05	9.3
<i>L — S01.3</i>	MCD	Bristol	5.2	1×10^{18}	2.25	0.62	11.95	10.8
<i>M — Photek tube</i>	MCD	Bristol	82(pk)	RD	-	-	-	-
<i>N — Gen 1</i>	MCD	GenVac	14(pk)		UK	NC	NC	NC

Sample D was initially measured as received from Diamond Detectors Limited, post polishing. This sample showed significant improvement after hydrogen re-termination, the peak SEE improving from 2.3 ± 0.3 to 11.0 ± 1.0 . After re-termination the SEE coefficient is comparable with the results of Yater et al. [2] at 0.5 kV (9.0 ± 0.2 over a $27\ \text{mm}^2$ area). However, in this sample and the majority of samples measured in the Leicester facility, we observe that the maximum of the SEE versus primary beam energy plot, SEE_{pk} , occurs at an energy, E_{SEEpk} , around 1 keV and in some cases < 0.5 kV (sample F in figure 4). This is significantly lower than reported elsewhere [2]. We have also observed a sample with an SEE_{pk} occurring at ~ 2 keV (sample N in figure 4), indicative that low SEE_{pk} values are not artefacts of the measurement technique, but more likely a characteristic of the material itself.

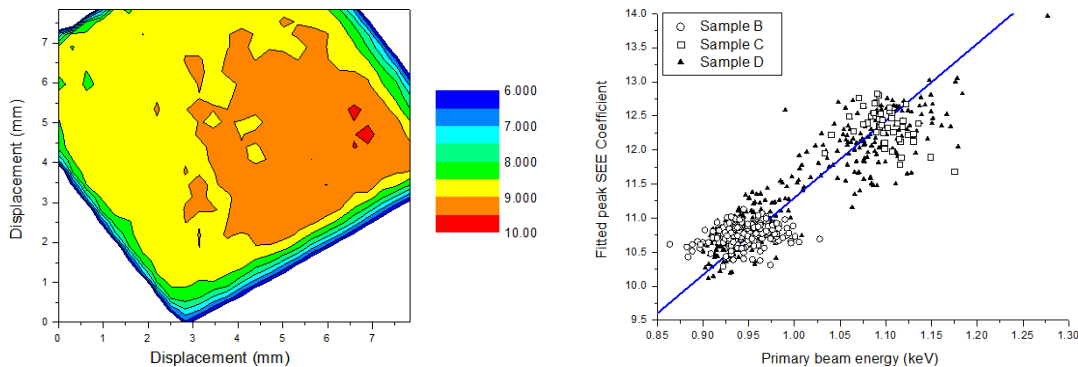


Figure 5. (a) A contour plot of SEE over sample D measured at 0.5 keV, and (b), a scatter plot of the SEE_{pk} fit versus $E_{SEE_{pk}}$, the variation in peak position (primary beam energy) with peak measured SEE coefficient at each pixel in contour plots for samples B, C, and D. A linear fit through the origin gives a gradient of 11.26(1), with a 0.67 R^2 value for all points.

4.1.1 SEE uniformity

DDL supplied samples, coated where required (samples A, B and C — see section 2.3), showed SEE coefficients at the high end of those measured and good uniformity. Sample, D, displayed an SEE coefficient of 11.5 over 26 mm², with a 12% standard deviation (abbreviated onwards as 11.5 \pm 1.4SD). A contour plot of the variation at 0.5keV over this sample is shown in figure 5a.

Areas of high SEE and good uniformity have also been observed on diamond grown at Bristol. For example sample J; 9.2 \pm 0.29SD over 9 mm² only a \sim 3% standard deviation.

The SEE_{pk} coefficient of sample D varies continuously over the sample as shown in figure 5a contour plot and figure 5b plot (triangles). The SEE_{pk} coefficient is more tightly grouped for sample B (plot 5b circles), the over-coated, unpolished polycrystalline diamond, or sample C (plot 5b squares), the polished, over-coated single crystal diamond.

The only samples with a polished surface investigated were A, C, and D, with A and C being over-coated with boron doped diamond. The SEE is uniform across the single crystal sample (C), but over the polycrystalline diamond (A) the SEE coefficient is low, and there is significant variation across the sample. Cross sections of the SEE through samples A, B, C and D at 0.5 keV are shown in figure 6.

The variation in SEE_{pk} over sample D is correlated with $E_{SEE_{pk}}$, figure 5b scatter plot. A similar but more extended correlation is shown across sample L figures 7a and 7b. Figures 5b and 7b are obtained by fitting the measured SEE at each pixel on the contour plot to the equation (4.1) [10] using the method outlined above.

4.1.2 Variation in sample thickness

In this work the boron concentrations in NCD and MCD films have been estimated from two point resistance measurements using the data and procedures reported in May [11], which shows correlation between resistance and SIMS determined boron concentrations. Note that the difference in film thickness between the films measured here and those used for correlation in [11] results in the boron concentration quoted being a “reasonable estimate”. In principle, the resistance measure-

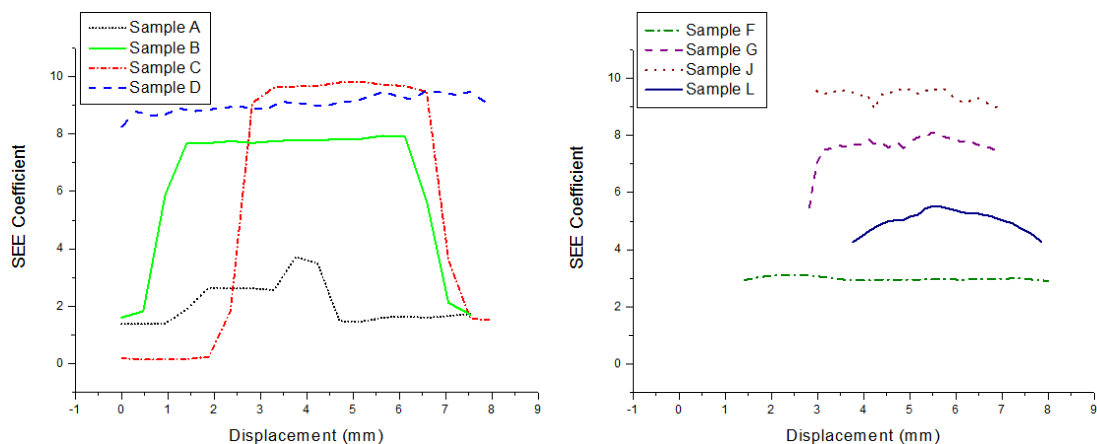


Figure 6. (a) Cross sections over SEE image maps of samples A, B, C and D. Measurements are taken at 0.5keV primary beam energy. (b) Cross sections over SEE image maps of samples F, G, J and L. Measurements are taken at E_{SEEpk} .

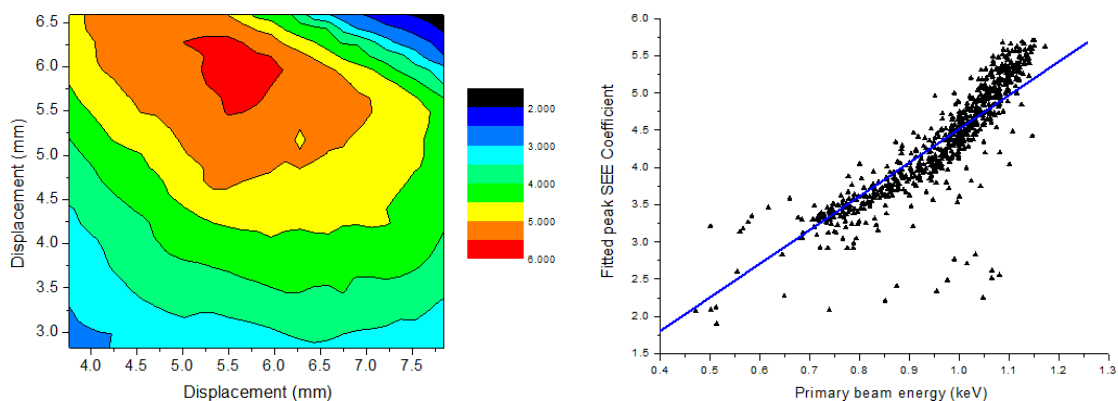


Figure 7. (a) Contour plot over sample L measured at 1.0keV. (b) Scatter plot showing the variation in SEE_{pk} with E_{SEEpk} at each pixel in the contour plot (a). In (b) a linear fit through the origin gives a gradient of $4.52(\pm 0.02)$, with a $0.76 R^2$ value for all points.

ments could be converted using known film thickness', however, for reasons outlined in [11] it is believed that such conversion would not improve the accuracy of these estimates.

Figure 8 hints at a reduction in SEE coefficient at high boron concentrations in MCD films. There is no observed variation in the SEE coefficient with boron concentration in NCD films. The SEE coefficient appears to vary with the thickness of NCD films, the thicker films producing a higher SEE_{pk} .

4.1.3 Test cell determined SEE coefficients

SEE coefficient measurements of hydrogen terminated polycrystalline diamond were simultaneously carried out at Photek within photo tubes (figure 2). SEE coefficients measured were similar to those obtained from the measurement facility at Leicester (~ 10). The SEE coefficients have been improved by a factor of 2–3 through vacuum baking.

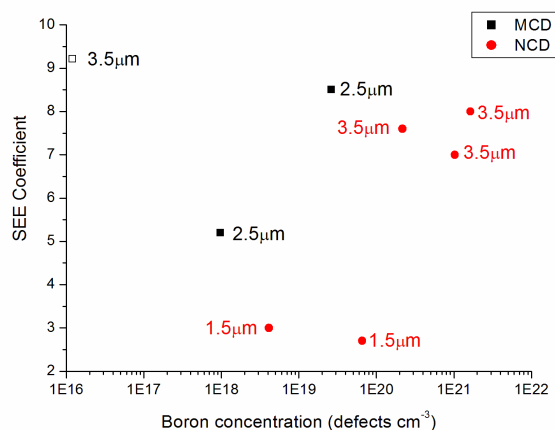


Figure 8. The average SEE coefficient measured over a selected area (see table 1), plotted against the calculated boron concentration. MCD samples are indicated by black squares and NCD samples by red circles. The film thickness is recorded next to each point. The open square indicates nominally zero boron concentration, but is placed at 1×10^{16} for clarity.

Further improvements were observed when the test-cell was manufactured into a sealed vacuum phototriode tube including an alkali metal based photocathode. SEE coefficients of up to 82 at 4 kV have been observed for sample M (see figure 4) with residual boron doping and a molybdenum substrate.

5 Discussion

5.1 Apparatus

The experimental apparatus and procedures described in sections 2 and 3 have proved to be an effective method of measuring the SEE coefficients over large areas as a measure of uniformity. By comparing results from different measurement techniques we estimate the error to be $\sim 10\%$. The spatial resolution of the SEE image depends on the electron beam footprint, however when using a small footprint, the increased current density causes the SEE to degrade more quickly. The SEM image in figure 9, which also images the SEE, shows where a single crystal sample has been aged by high current density over an array of measurement points. The pattern spots are stretched in one axis due to the small variation in the beam position with different primary beam energies, and the bright portion on the left shows where the sample has not been tested. The darker regions remain unexplained.

The general improvement in SEE in the original samples which were re-terminated with hydrogen and transported in contamination controlled containers backfilled with dry nitrogen indicates both diamonds sensitivity to surface contamination but robustness with respect to exposure to (clean) atmosphere. The poor performance of sample A after re-termination may be due to existing polishing damage which can impact termination quality [11].

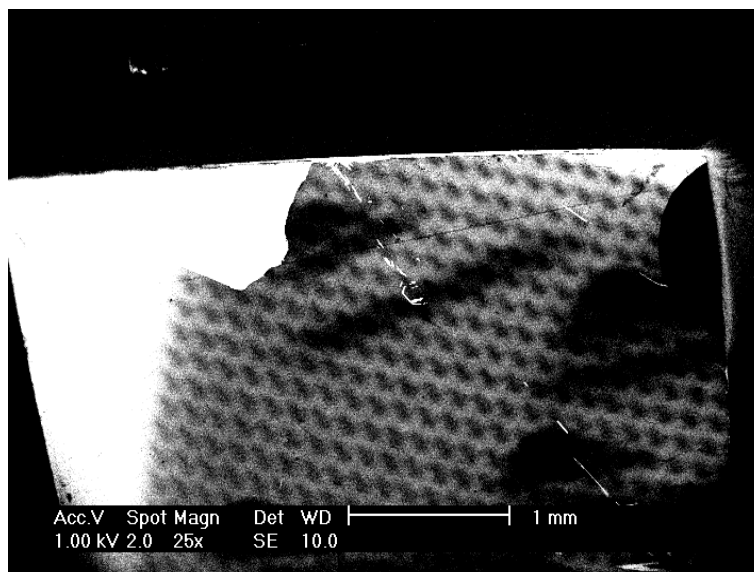


Figure 9. An SEM image illustrating the effect of measurement over an array of points, causing reduced SEE, and small positional shifts of the electron beam with beam energy.

5.2 Low peak SEE energy

We have previously reported SEE coefficients up to 45 [6]. These measurements represented the best single spot measurements obtained in pulsed beam mode at low current to minimize ageing and charge-up concerns. Since these measurements, the experimental setup and procedures have been refined, but measurements with the same sample have not proved repeatable. Experimental error, such as loss of secondary electrons in the case where the total measured current is used to represent the beam current, could be the cause of inflated SEE values. However our initial measurements were performed with an LFC bias of +400V which should preclude this effect, however the discrepancy between the two sets of results remains unresolved.

Our recent SEE measurements have generally exhibited SEE_{pk} of around 10-15 with an E_{SEEpk} of ~ 1 keV (although one sample, N, has been observed with an $E_{SEEpk} \sim 2$ keV). Even after refinement of handling procedure and re-termination (of all but the Gen1 sample), this is substantially lower than the best reported by Yater et al. [2]. We suspect that our results are influenced by; incomplete termination and/or surface contamination, and possibly high dopant concentration which is not well characterized.

Lower E_{SEEpk} are reported where measurements are made after exposure to the atmosphere without subsequent heat treatment [13] and higher peak positions observed post heat treatment. It is reasonable to assume that this removes hydrocarbon contaminants reducing the height of the vacuum barrier.

All samples reported on here have been exposed to similar laboratory and transport conditions, so it seems unlikely that the contamination level on sample N, which shows a higher peak position, differs significantly. However, the presence of surface contamination on our samples is supported by evidence from parallel measurements at Photek Ltd., who have characterized diamond samples from the same manufacturing batches in vacuum tubes. These have consistently shown higher SEE_{pk} and E_{SEEpk} . All tube components undergo over night bake-out above 200 °C and are ex-

posed to photocathode precursor chemicals, which include various alkali metals. It seems likely that improved SEE in these tubes results from (i) the heat treatment removing surface contaminants, and (ii) serendipitous surface termination by alkali metals producing NEA enhancement.

Other than surface contamination effects, lower than expected SEE_{pk} and E_{SEEpk} could be linked to high dopant concentration, since electron-dopant scattering dominates for low energy secondary electron transport. However we cannot estimate boron concentration for the most promising samples (Sample N and M) since they are deposited on Molybdenum substrates, invalidating the 2 or 4 point probe resistance measurement. The boron concentration for all samples on silicon has been measured using 2 and 4 point probe measurements, however the model used for this [11] assumed undoped silicon. Since we used p-type conductive silicon to allow back contact of the material, it is likely that all boron concentrations are over estimated, though relative concentrations may still be valid.

We observed increasing SEE with film thickness on NCD material. This is presumed to be due to increasing crystal size with film thickness. Feasibly, the higher grain boundary density in NCD could reduce SEE due to higher probability of losses at grain boundaries, however samples A, B and D which have large $\sim 50 \mu\text{m}$ grains still showed a lower E_{SEEpk} .

Both samples producing the highest measured SEE coefficients, figure 4 (samples M and N) were grown on Molybdenum substrates, however as yet we have too little data to draw firm conclusions from this.

5.3 SEE uniformity

We have measured uniform SEE coefficients over areas up to 26 mm^2 with values of $11.5 \pm 1.4SD$, on commercially grown (Element Six, Diamond Detectors Limited provided) polycrystalline diamond with $\sim 50 \mu\text{m}$ grain size (sample D). SEE coefficients of $9.2 \pm 0.3SD$ over smaller areas, $\sim 10 \text{ mm}^2$, on diamond grown at Bristol University have been observed. Similar uniformities have been reported elsewhere [2].

In a practical photomultiplier operating with a first dynode mean gain of n , the intrinsic gain variation will vary as \sqrt{n} , or 20% at a gain of 25, so an intrinsic variation of dynode gain 12% or less is reasonable for a multi-stage device.

Differences in uniformity and SEE_{pk} between sample A (polished polycrystalline) and sample B (unpolished polycrystalline) are likely to result from the polishing process, possibly the result of varied diamond growth rates, or even selective etching [14] on different polished crystal grains. The same affect is not observed on sample C, the single crystal sample, because the growth face is consistent over the sample and close to [001] providing a consistent surface for diamond growth. Sample B, with an unpolished polycrystalline surface, shows a good and uniform SEE coefficient as expected if the over-coated diamond builds on surface facets from the previous growth process.

5.4 Boron concentration

Diamond films have been grown on p-type conducting silicon and molybdenum substrates, making it difficult to conclusively assign the boron concentration from resistivity measurements as in [11]. However, the resistance measurements are similar to those reported in [11] using the same growth equipment and chemistries. As a result we expect our absolute concentrations to be inflated

though the relative concentrations between samples of equal thickness are likely to be reasonable estimates.

5.5 Sample thickness

The most obvious trend emerging from data presented here is the increase SEE_{pk} with increasing film thickness for nano-crystalline diamond films (figure 8). It is well known that crystal size in CVD deposited polycrystalline diamond increases with sample thickness [15], particularly when the process is optimised for columnar growth as used here. Since our electron beam spot size is too large to probe individual grains, the likelihood of primary electrons scattering loss at the grain boundary, resulting in lower SEE_{pk} will depend on the grain boundary density. Thus we might expect that this effect is more prevalent in NCD material where the grain boundary density is higher. This result may limit the potential SEE for transmission configurations which will require membranes $\ll 0.5 \mu\text{m}$ thick for primary electron energies available at realistic operating voltages.

It is possible that with NCD material the grain boundaries are the dominant scattering mechanism and thus high boron concentrations will not have the same detrimental effect. However, our current data does not conclusively confirm this.

5.6 Test cell measurements

Test cell measurements at Photek have produced an SEE_{pk} of 82 for a polycrystalline hydrogen terminated diamond. Such SEE coefficients are not unrealistically high. Shih et al. [1] report 84 at 3 kV, but Cs terminated surfaces are more likely to yield such SEE coefficients [16]. Given the improvement in SEE coefficient when incorporated in a test-cell process involving bake-out and photocathode manufacture, it is possible that mobile alkali metal photocathode precursor materials terminate the diamond surface, improving the SEE beyond that expected if surface decontamination was the only beneficial action. The test cell process temperatures may be fortuitous, resulting in a heating cycle close to the 200°C required to remove excessive Cs clusters as suggested by [17]. It is not clear if test cell manufacturing process is sufficient to re-terminate the sample but it certainly appears to have a significant effect on the SEE coefficient.

6 Conclusions

The measurement of Secondary electron emission, especially from high gain materials, is not as straightforward as might be initially anticipated. We have refined an experimental facility and processes used to characterize CVD diamond for application to photomultiplier dynodes, improving measurement accuracy and repeatability by design and operational modifications. The facility has been used to image SEE versus primary electron energy over extended samples to measure uniformity, sensitivity to dopant concentration, film thickness, and crystallite grain size. While SEE values measured remain lower than desired (an average maximum of 12.3 reported here) uniformity with an impressive standard deviation of 3% has been seen. Inconsistent results from nominally similar materials is a theme through the data, however though there have been few strong trends, the improvement of SEE with increasing film thickness and with surface termination quality are notable exceptions. The SEE measurements of samples from the same batch mounted in vacuum test cells show improvement of between 2–6, indicating the strong sensitivity of diamond to surface contamination and termination. In this case, processing temperatures and materials undoubtedly

decontaminate and possibly re-terminate the diamond surface. Measurements on a larger set of samples, including the dependence on primary beam incident angle, temporal SEE variation, and operation at elevated temperature are also in progress and will be published in a future report.

Acknowledgments

The authors would like to thank Kevin Oliver of Diamond Detectors Limited for loan of a variety of diamond test samples manufactured by Element 6, our collaborators at the University of Bristol and RAL for the provision and preparation of CVD diamond samples, and David Scurr at the University of Nottingham for his help with SIMS characterisation. This work was supported by funding from the Science and Technology Facilities Research Council and the Atomic Weapons Establishment.

References

- [1] A. Shih et al., *Secondary electron emission from diamond surfaces*, *J. Appl. Phys.* **82** (1997) 1860.
- [2] J.E. Yater, A. Shih and R. Abrams, *Electron transport and emission properties of diamond*, *J. Vac. Sci. Tech. A* **16** (1998) 913.
- [3] *Photonis PMT handbook*.
- [4] *PSP Vacuum Technology*, Macclesfield, U.K., <http://www.pspvacuum.com>.
- [5] P.W. May, *Diamond thin films: a 21st-century material*, *Phil. Trans. Roy. Soc. Lond. A* **358** (2000) 473.
- [6] J.S. Lapington et al., *Investigation of the secondary emission characteristics of CVD diamond films for electron amplification*, *Nucl. Instrum. Meth. A* **610** (2009) 253.
- [7] J.B. Cui et al., *Hydrogen termination and electron emission from CVD diamond surfaces: a combined secondary electron emission, photoelectron emission microscopy, photoelectron yield, and field emission study*, *Diam. Relat. Mater.* **9** (2000) 1143.
- [8] H.J. Hopman et al., *Secondary electron emission measurements on synthetic diamond films*, *Diam. Relat. Mater.* **8** (1999) 1033.
- [9] D. Briggs, *Analysis of polymer surfaces by SIMS — 3. Preliminary results from molecular imaging and microanalysis experiments*, *Surf. Interface Anal.* **5** (1983) 113.
- [10] A.J. Dekker, *Secondary electron emission*, Academic Press, New York, U.S.A. (1958), see pp. 251–315.
- [11] P.W. May et al., *Raman and conductivity studies of boron-doped microcrystalline diamond, faceted nanocrystalline diamond and cauliflower diamond films*, *Diam. Relat. Mater.* **17** (2008) 105.
- [12] D.P. Malta et al., *Surface damage effects on secondary electron emission from the negative electron affinity diamond surface*, *Mat. Res. Soc. Symp. Proc.* **416** (1996) 311.
- [13] J.B. Miller and G.R. Brandes, *Effects of dopant concentration, crystallographic orientation, and crystal morphology on secondary electron emission from diamond*, *J. Appl. Phys.* **82** (1997) 4538.
- [14] M. Wolfer et al., *Crystallographic anisotropy of growth and etch rates of CVD diamond*, *Diam. Relat. Mater.* **18** (2009) 713.
- [15] J.E. Graebner et al., *Unusually high thermal conductivity in diamond films*, *Appl. Phys. Lett.* **60** (1992) 1576.
- [16] J.E. Yater and A. Shih, *Secondary electron emission characteristics of single-crystal and polycrystalline diamond*, *J. Appl. Phys.* **87** (2000) 8103.

- [17] A. Shih and J.E. Yater, *Properties of secondary electron emission from diamond: influence of surface*, in *Properties, growth and applications of diamond*, M.H. Nazare and A.J. Neves eds., INSPEC Inc. (2000).

2012 JINST 7 C03018